Nanocrystal Structures

DOI: 10.1002/anie.201004502

Chemical Imaging at Atomic Resolution as a Technique To Refine the Local Structure of Nanocrystals**

Susana Trasobares, Miguel López-Haro, Mathieu Kociak, Katia March, Francisco de La Peña, Jose A. Perez-Omil, Jose J. Calvino, Nathan R. Lugg, Adrian J. D'Alfonso, Leslie J. Allen, and Christian Colliex*

Dedicated to Professor Serafin Bernal on the occasion of his retirement

The challenging problem of mapping the chemical composition of cation columns in individual nanocrystals at atomic resolution is addressed by using a method based on aberration-corrected electron microscopy, core-loss electron energy-loss spectroscopy, and simulations. The potential of this novel approach to provide unique structural information, which is the key to rationalizing macroscopic behavior, is illustrated with the analysis of ceria–zirconia mixed oxides, which are nanomaterials with substantial technological impact.

Metal nanoparticles supported on this family of oxides are currently materials of interest as catalysts in a variety of chemical transformations in the area of environmental protection, such as low-temperature water-gas shift, selective oxidation of CO in the presence of large amounts of hydrogen, or three-way catalysis. Strong variations in the chemistry of ceria–zirconia mixed oxide catalysts have been observed after they have undergone redox cycles involving reduction treatments at high temperatures (≥ 1173 K) then oxidation at mild temperatures (≤ 823 K).[1,2] In particular their reducibility is significantly enhanced[3–6] after such aging treatments.

Scanning transmission electron microscopy (STEM) techniques have provided crucial information to account for these changes in the redox behavior.[7,8] High-resolution electron microscopy (HREM) combined with high-angle annular dark-field (HAADF) imaging and tomography have revealed the occurrence of a disorder–order transformation in the cationic sublattice of these oxides, which tend to rearrange into a distribution characteristic of the so called pyrochlore phase. This phase is an archetype structure for $A_2B_2O_7$ (A = +3 cation, B = +4 cation) compounds and can be considered a fluorite superstructure. The structural transformation takes place during the reduction step of the cycle, in which the fully reduced mixed oxide with Ce/Zr molar ratio 1:1 adopts the $Ce_2Zr_2O_7$ stoichiometry. Nevertheless, HAADF studies have clearly shown that, in the case of ceria–zirconia mixed oxides, this cation-ordered arrangement is preserved even after full reoxidation, that is, in the oxide with $Ce_2Zr_2O_8$ stoichiometry, whenever the oxidation temperature does not exceed 823 K.[8]

Electron-microscopy studies have also revealed[9–11] another remarkable feature of the ceria–zirconia aged oxides with the pyrochlore-type cation sublattice: the occurrence of compositional heterogeneities at the nanometer scale. Taking these observations into account and also considering that the disorder–order transition may not be completed in the time scale and under the temperature conditions used in the redox-cycling treatments, the important question arises whether these heterogeneities are in fact occurring on a finer scale, that is, at the atomic level. Such heterogeneities, compatible with the HREM and HAADF observations, will strongly influence the details of the counterpart oxygen sublattice and, consequently, the chemical and catalytic response of these oxides.

To date, the atomic-column by atomic-column compositional analysis of the oxidized pyrochlore required to justify such a possibility has not been accomplished. Herein, using the capabilities of an aberration-corrected Nion UltraSTEM microscope (operated at 100 kV) we not only provide the first direct chemical evidence of the cationic order present in the $Ce_2Zr_2O_8$ oxidized pyrochlore but we also show how atomic-resolution electron energy-loss spectroscopy (EELS) mapping, based on core–shell ionization, can be combined with EELS image simulation[12] to detect quite subtle local deviations in the cation sublattice from the completely ordered structure. This information provides a much more accurate structural description of the active catalyst nanocrystals, which must be considered to model both their oxygen-exchange capabilities and, eventually, their catalytic performance.

[*] Dr. S. Trasobares, Dr. M. López-Haro, Dr. J. A. Perez-Omil, Dr. J. J. Calvino
Departamento de Ciencia de los Materiales e Ingeniería Metalúrgica y Química Inorgánica
Facultad de Ciencias, Universidad de Cádiz
Campus Rio San Pedro, 11510-Puerto Real, Cádiz (Spain)
Fax: (+34) 956-016286
E-mail: susana.trasobares@uca.es
Homepage: http://www.uca.es/tem-uca
Dr. M. Kociak, Dr. K. March, Dr. F. de La Peña, Prof. C. Colliex
Laboratoire de Physiques des Solides UMR 850
Université Paris Sud, 91405 Orsay (France)
N. R. Lugg, Dr. A. J. D'Alfonso, Prof. L. J. Allen
School of Physics, University of Melbourne
Victoria 3010 (Australia)

[**] We acknowledge the financial support from Spanish MICINN/FEDER-EU (Project MAT2008-00889-NAN and CSD2009-00013), the Junta de Andalucia (Proyectos de Excelencia FQM-02433), and from the European Union under the Framework 6 program under a contract for an Integrated Infrastructure Initiative, Reference 026019 ESTEEM. L.J.A. acknowledges support by the Australian Research Council.

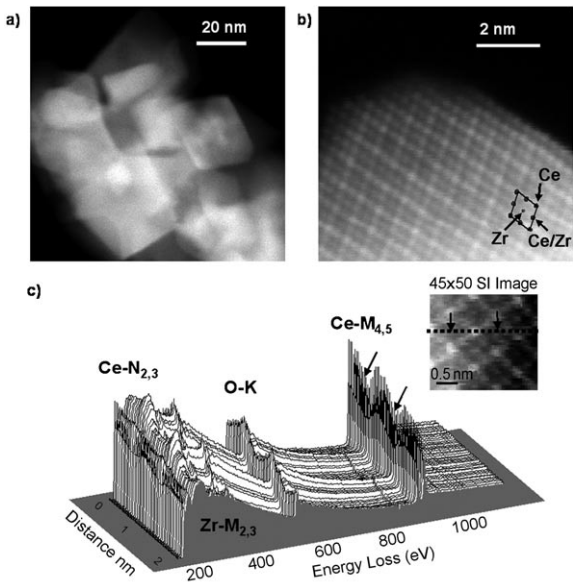

Figure 1. Atomic-resolution spectrum-imaging (SI) analysis on an individual nanocrystal. a) HAADF image of the $Ce_2Zr_2O_8$ sample. b) High-resolution HAADF image of a nanocrystal showing the superstructure as described in the model proposed in Ref. [8]. c) 3D plot of the EELS spectra extracted from the spectrum imaging. Inset: the simultaneously acquired HAADF signal. The 3D EELS data have been extracted from the line shown, which passes along the two different positions in the structure of the ideal pyrochlore structure (above a column containing only Ce atoms, above a column containing only Zr atoms). The positions marked with arrows are explained in the text.

A medium magnification HAADF image of a $Ce_2Zr_2O_8$ sample (Figure 1a) shows an agglomeration of crystals 20–30 nm in size, which do not have any specific orientation or thickness. To elucidate the chemical features of the cationic order of a nanocrystal with the pyrochlore structure, the investigation focused on individual crystals at the surface of the agglomerate. Furthermore, within a selected crystal a relatively thin area has been chosen for analysis. As described in Ref. [8], the ideal pyrochlore structure gives rise to three distinct types of cationic columns in the [110] projection: pure Ce columns (which in this projection occur on the vertices of a rhombus (overlay Figure 1b)), pure Zr columns located at the center of the rhombus, and mixed Ce–Zr columns half way along the edge of the rhombus. We will use this rhombus to reference the position of an atomic column in this projection of the ideal oxidized pyrochlore structure. Likewise we will refer to the situation in which these three kinds of atomic columns can be identified in the [110] projection as the "ideal pyrochlore structure". Figure 1b shows a high-resolution HAADF image of the $Ce_2Zr_2O_8$ nanocrystal on which the analysis has been carried out. Aberration corrected STEM EELS provides a useful tool to analyze the chemical composition of the superstructure and also to reveal the structure of the crystal. For our specimen the characteristic signals derived from the Ce-$N_{2,3}$, Zr-$M_{2,3}$, O-K, and Ce-$M_{4,5}$ edges are present at 207, 330, 530, and 881 eV, respectively, see Figure 1c. Ideally, the desired situation is that there is a direct correlation between the image constructed from these spectra as a function of probe position and the structure of the specimen. However, signals can be obtained from columns that are not immediately under the beam as a result of the long-range nature of the ionization transition potentials coupled with the effects of thermal scattering.[12,13]

The spectrum-imaging mode has been used to characterize the area indicated in the inset in Figure 1c. This technique consists of simultaneously acquiring EELS and HAADF signals while scanning a probe of nominally 1 Å full-width at half-maximum over a defined area of the crystal (2.44 nm × 2.16 nm). The matrix of spectra, called a spectrum-image, is then de-noised using standard principal component analysis (PCA),[14] and the chemical maps are constructed using a power-law background subtraction.[15] Figure 1c shows the acquired HAADF signal (inset) as well as a series of 40 spectra, extracted from the spectrum imaging data, along a line across two rhombi on the superstructure. The characteristic signals of Ce-$N_{2,3}$, Zr-$M_{2,3}$, O-K, and Ce-$M_{4,5}$ transitions are present in the 3D plot. A variation of the Ce-$M_{4,5}$ signal is observed through the rhombus, a minimum in the Ce-$M_{4,5}$ signal is observed when the probe is located at the center of the rhombus (see arrows).

Atomic-resolution Ce-$M_{4,5}$ and Zr-$M_{2,3}$ chemical maps (Figure 2) illustrate for the first time, direct chemical evidence of a cationic order in a $Ce_2Zr_2O_8$ nanocrystal. In particular, the maximum signals for Ce and Zr are found at the vertices

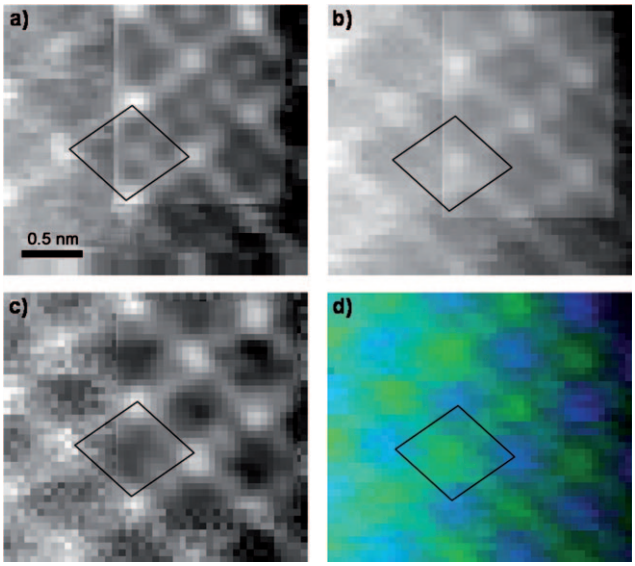

Figure 2. Atomically resolved chemical information on an individual nanocrystal. a) HAADF signal acquired simultaneously with the EELS signal, b) Zr-$M_{2,3}$, and c) Ce-$M_{4,5}$ atomic-resolution chemical maps obtained on a (nominally) $Ce_2Zr_2O_8$ nanocrystal. Inset images correspond to the experimental data after applying a low-pass filter. d) Experimental Zr (green) and Ce (blue) composite map.

and center of the marked rhombus, respectively, as expected for this projection of the ideal pyrochlore structure. It is important to note the presence of Zr signal on the vertices of the rhombus (see below), signal which is not expected for this ideal structure.[8]

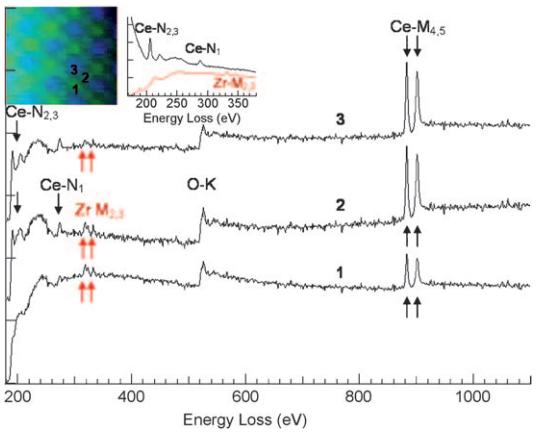

Figure 3. EELS spectra extracted at the three different positions (based on the ideal pyrochlore structure[8] from the atomic resolution chemical map; those which correspond to a nominally pure Zr column (1), a mixed Ce–Zr column (2), and a nominally pure Ce column (3). Insets: illustrate the area from which the spectra have been extracted and Ce and Zr EELS spectra taken from reference samples.[16]

EELS spectra extracted from three different positions: pure Zr column (Figure 3 position 1), mixed Ce–Zr column (Figure 3 position 2), and pure Ce column (Figure 3 position 3) indicate the presence of signals characteristic for Zr-$M_{2,3}$, O-K, and Ce-$M_{4,5}$. Looking in detail at the fine structure of the spectrum in the 180–360 eV range and comparing it with those found on Ce and Zr oxide reference samples[16] (inset, Figure 3), we observe that signals characteristic for Ce-$N_{2,3}$, Ce-N_1, and Zr-$M_{2,3}$ are present in spectra 2 and 3, while neither of the Ce-N signals is visible in spectrum 1. It is also important to note the presence of Ce-$M_{4,5}$ in spectrum 1, whereas the ideal pyrochlore structure suggests the presence of only Zr in such a position.

A detailed analysis of the atomic-resolution EELS mapping has to take into account the spreading and dechanneling of the probe in the crystal as well as the delocalization of the ionization interaction.[17] Therefore to clarify the experimental results and to obtain quantitative information about the ordering of atoms in the sample, EELS image simulation has been performed using four different structural models: A) a crystal presenting the "ideal pyrochlore structure", B) a crystal where a certain amount of Zr has replaced Ce atoms in the "ideal pyrochlore structure", C) a crystal where a certain amount of Ce has replaced Zr atoms in the "ideal pyrochlore structure", and D) a crystal presenting a small fraction of cationic disorder in its structure. Of the listed structures, (B) and (C) correspond to a compositional variation and (D) to a disordered structure. Simulations were performed using the Bloch wave method with an effective ionization potential.[18] A specimen thickness of 20 nm was used to calculate Ce-$M_{4,5}$ and Zr-$M_{2,3}$ chemical maps for the four different models.

In the case of model (A), the "ideal pyrochlore structure" (Figure 4a), the maximum Ce signal is found at the vertices of the rhombus while the peak signal corresponding to Zr is located at its center (as expected from the structure). We note

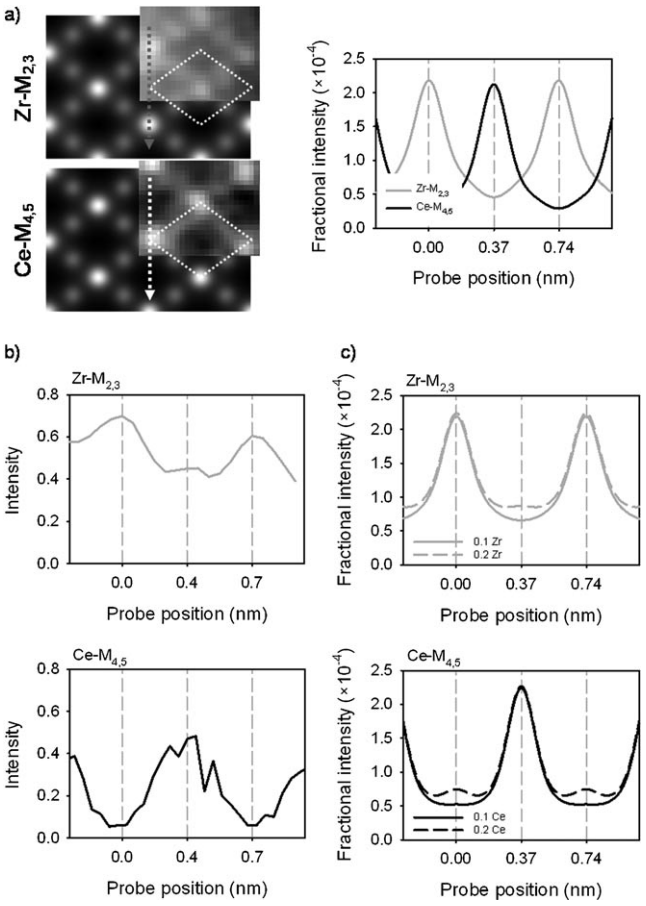

Figure 4. Simulated chemical maps. a) Theoretical simulations for the Zr-$M_{2,3}$ and Ce-$M_{4,5}$ edges are shown for the "ideal pyrochlore structure",[8] with sections of the experimental images overlaid. Line scans are shown along the generic $[1\bar{1}0]$ direction as indicated by the broken arrows. b) Experimental Zr-$M_{2,3}$ (top) and Ce-$M_{4,5}$ (bottom) line scans, also in the generic $[1\bar{1}0]$ direction. c) Simulated Zr-$M_{2,3}$ (top) and Ce-$M_{4,5}$ (bottom) maps of modifications of the "idea pyrochlore structure" made by incorporating Zr in the pure Ce columns (0.10 and 0.20 occupancy) and by incorporating Ce in the pure Zr columns (0.10 and 0.20 occupancy).

that the intensity profiles along the $[1\bar{1}0]$ direction in Figure 4a show a background signal which can be related to the interaction delocalization and beam broadening through the sample (Figure 4a).[12,13] When comparing the experimental Zr signal (Figure 4b) with the simulated one (Figure 4a) a clear discrepancy is observed on the vertices of the rhombus, in such a position there is a signature for Zr in the experimental map (at probe position 0.4 nm) while the Zr signal is absent in the simulated one. Therefore the proposed "ideal pyrochlore structure" for the nanocrystal[8] is not adequate at that specific point and needs to be modified to obtain agreement with the experimental results. In model (B) described above, a fractional amount of Zr is incorporated on positions occupied by Ce in the "ideal pyrochlore structure". Figure 4c illustrates the Zr simulated intensity profiles when Zr has a fractional occupancy of 0.10 and 0.20 on nominally Ce sites. A qualitative comparison between the experimental image (Figure 4b) and the simulated ones (Figure 4c),

suggests that the replacement of approximately 0.20 of Ce by Zr is occurring. Such a result implies that the nanocrystal has a composition which diverges from the nominal stoichiometry with equal amounts of Ce and Zr. To confirm this model and also to eliminate the possibility of cationic disorder in the sample, similar simulations have been performed for the two additional models (C) and (D). Simulated data obtained for model (C) clearly indicates that a fractional occupancy of 0.20 Ce on nominally Zr sites gives rise to a bump in the line profiles of the Ce maps which peaks at the location of the Zr columns in the "ideal pyrochlore structure". This situation however is not consistent with the experimental data in Figure 4b, as can be seen in Figure 4c. For model (D), similar results (not shown) are obtained for the Ce map to those in model (D), which also invalidates this model. We have also performed simulations to eliminate the possibility that the Zr signal above the background on the Ce column is due to thermal scattering of electrons onto adjacent Zr columns using a Born–Oppenheimer type model for phonon excitation.[19] Therefore, we can conclude that, for the nanocrystal analyzed in this experiment, there is a preferential substitution of Ce by Zr, which implies a local compositional variation which suggests Ce/Zr molar ratios in the 45:55 and 40:60 range.

These results demonstrate the feasibility of a new method to obtain chemical and structural information on catalytic nanoparticles. For the first time EELS has not only provided 2D atomic-resolution chemical information about nanocrystals. The approach has allowed us to discriminate between a local deviation in stoichiometry and a purely partial-disorder effect. In particular, it has revealed a local deviation of the structure from that of the expected ideal pyrochlore, which is linked to a preferential substitution by Zr^{4+} ions at the positions of the Ce^{4+} in the perfect structure. Such local chemical composition deviations within the cation network are of utmost importance with regard to the structure of the complementary oxygen sublattice.

To conclude, 2D atomic-resolution chemical maps have been experimentally obtained for a Ce–Zr mixed oxide nanocrystal. A methodology which combines HAADF and experimental and simulated EELS mapping has been used to analyze, with atomic column resolution, the structure and composition of an individual nanocrystal. Our findings indicate that in the catalyst showing enhanced redox performance, obtained after redox-cycling treatments local compositional deviations at the atomic scale are present in the nanocrystal. These results are at variance with the previously proposed "ideal pyrochlore structure" for the material. This new information needs to be considered when correlating the chemical activity of high-temperature aged cerium–zirconium mixed oxides and their catalytic performance. Finally, with the approach used herein, the analysis of other very challenging characterization problems, such as the composition of surfaces of nanocrystals or those of metal/oxide nanointerfaces, are in reach.

Experimental Section

The nominal $Ce_2Zr_2O_8$ sample, kindly provided by Rhodia, was submitted to a reduction treatment under a 500 $cm^3 min^{-1}$ H_2 (5% Ar) flow at 1223 K for 1 h then a 60 $cm^3 min^{-1}$ flow of He for 1 h. After cooling the sample to 298 K in an inert atmosphere, it was submitted to a series of re-oxidation processes, first at 298 K with O_2 pulses until no further consumption was observed, and later by heating under flowing O_2 (5%)/He at 773 K for 1 h.

The electron microscopy sample grid was prepared by depositing a small amount of the sample powder directly onto holey-carbon coated Cu grids. Excess powder was removed from the grids by gentle blowing with a nozzle.

Spectrum imaging analysis was performed on a NION UltraSTEM microscope operated at 100 kV and corrected up to fifth-order aberrations. To compensate for possible sample drift during the analysis, a spatial drift correction was used on every line of the analysis. Every spectrum was acquired using an acquisition time of 20 ms and an energy dispersion of 1 eV per channel. Spectrum-images were recorded using 35 mrad and 80 mrad convergence and collection semi-angles, respectively. The recorded data was treated by PCA and independent components analysis[14,20] to de-noise and estimate the number of components. Zr and Ce chemical maps were obtained by analyzing the $M_{2,3}$ Zr signal (320–360 eV) and the $M_{4,5}$ Ce signal (876–916 eV).

The Bloch wave simulations assumed an aberration-free probe with a convergence semi-angle of 35 mrad. The EELS detector collection angle was modeled as subtending a semi-angle of 80 mrad. To account for the demagnification of the electron source, which is necessary for the high probe currents used, the effect of the probe spatial incoherence was accounted for by the convolution of the images with a Gaussian of full width at half maximum (FWHM) 0.15 nm.[21] This number permitted the best visual comparison with experiment across all spectroscopic images.

Received: July 22, 2010
Revised: October 21, 2010

Keywords: ceria–zirconia · EELS · mixed oxides · nanocrystals · scanning probe microscopy

[1] P. Fornasiero, G. Balducci, R. DiMonte, J. Kaspar, V. Sergo, G. Gubitosa, A. Ferrero, M. Graziani, *J. Catal.* **1996**, *164*, 173.
[2] A. Trovarelli, *Catal. Rev. Sci. Eng.* **1996**, *38*, 439.
[3] R. T. Baker, S. Bernal, G. Blanco, A. M. Cordon, J. M. Pintado, J. M. Rodriguez-Izquierdo, F. Fally, V. Perrichon, *Chem. Commun.* **1999**, 149.
[4] N. Izu, T. Omata, S. Otsuka-Yao-Matsuo, *J. Alloys Compd.* **1998**, *270*, 107.
[5] H. Kishimoto, T. Omata, S. Otsuka-Yao-Matsuo, K. Ueda, H. Hosono, H. Kawazoe, *J. Alloys Compd.* **2000**, *312*, 94.
[6] S. Otsuka-Yao-Matsuo, T. Omata, N. Izu, H. Kishimoto, *J. Solid State Chem.* **1998**, *138*, 47.
[7] J. C. Hernandez, A. B. Hungria, J. A. Perez-Omil, S. Trasobares, S. Bernal, P. A. Midgley, A. Alavi, J. J. Calvino, *J. Phys. Chem. C* **2007**, *111*, 9001.
[8] J. A. Pérez-Omil, S. Bernal, J. J. Calvino, J. C. Hernandez, C. Mira, M. P. Rodriguez-Luque, R. Erni, N. D. Browning, *Chem. Mater.* **2005**, *17*, 4282.
[9] M. P. Yeste, J. C. Hernandez, S. Trasobares, S. Bernal, G. Blanco, J. J. Calvino, J. A. Perez-Omil, J. M. Pintado, *Chem. Mater.* **2008**, *20*, 5107.
[10] R. G. Wang, P. A. Crozier, R. Sharma, J. B. Adams, *J. Phys. Chem. B* **2006**, *110*, 18278.
[11] J. Hernandez-Garrido, *PhD Thesis*, Cadiz University, **2007**.

[12] M. Bosman, V. J. Keast, J. L. Garcia-Munoz, A. J. D'Alfonso, S. D. Findlay, L. J. Allen, *Phys. Rev. Lett.* **2007**, *99*, 086102.
[13] P. Wang, A. J. D'Alfonso, S. D. Findlay, L. J. Allen, A. L. Bleloch, *Phys. Rev. Lett.* **2008**, *101*, 236102.
[14] N. Bonnet, N. Brun, C. Colliex, *Ultramicroscopy* **1999**, *77*, 97.
[15] R. F. Egerton, *Electron Energy-Loss Spectroscopy in the Electron Microscope*, Plenum, New York, **1996**.
[16] C. C. Ahn, *Transmission Electron Energy Loss Spectrometry in Materials Science and the EELS Atlas*, Wiley-VCH, Weinheim, **2004**.
[17] C. Dwyer, J. Etheridge, *Ultramicroscopy* **2003**, *96*, 343.
[18] L. J. Allen, S. D. Findlay, M. P. Oxley, C. J. Rossouw, *Ultramicroscopy* **2003**, *96*, 47.
[19] B. D. Forbes, A. V. Martin, S. D. Findlay, A. J. D'Alfonso, L. J. Allen, *Phys. Rev. B* **2010**, *82*, 104103.
[20] M. R. Keenan, P. G. Kotula, *Surf. Interface Anal.* **2004**, *36*, 203.
[21] P. D. Nellist, J. M. Rodenburg, *Ultramicroscopy* **1994**, *54*, 61.

